

# Structural Basis of Rho GTPase-Mediated Activation of the Formin mDia1

Takanori Otomo, Chinatsu Otomo,  
Diana R. Tomchick, Mischa Machius,  
and Michael K. Rosen\*  
Department of Biochemistry  
University of Texas Southwestern  
Medical Center at Dallas  
5323 Harry Hines Boulevard  
Dallas, Texas 75390

## Summary

Diaphanous-related formins (DRFs) regulate dynamics of unbranched actin filaments during cell contraction and cytokinesis. DRFs are autoinhibited through intramolecular binding of a Diaphanous autoinhibitory domain (DAD) to a conserved N-terminal regulatory element. Autoinhibition is relieved through binding of the GTPase RhoA to the N-terminal element. We report the crystal structure of the dimeric regulatory domain of the DRF, mDia1. Dimerization is mediated by an intertwined six-helix bundle, from which extend two Diaphanous inhibitory domains (DIDs) composed of five armadillo repeats. NMR and biochemical mapping indicate the RhoA and DAD binding sites on the DID partially overlap, explaining activation of mDia1 by the GTPase. RhoA binding also requires an additional structurally independent segment adjacent to the DID. This regulatory construction, involving a GTPase binding site spanning a flexibly tethered arm and the inhibitory module, is observed in many autoinhibited effectors of Ras superfamily GTPases, suggesting evolutionary pressure for this design.

## Introduction

Signal-mediated rearrangements of the actin cytoskeleton often require generation of new actin filaments. Three cellular nucleation factors have been discovered that are downstream targets of many signaling pathways. Arp2/3 complex nucleates filaments that grow from the sides of existing filaments, leading to branched networks (Carlier et al., 2003; Higgs and Pollard, 2001; Weaver et al., 2003) that are necessary for motility, polarization, and organelle and pathogen movement in a wide range of cell types (Fehrenbacher et al., 2003; Miletic et al., 2003; Pollard and Borisy, 2003). Members of the large family of formin proteins nucleate unbranched filaments that are bundled into structures integral to yeast actin cables, actin stress fibers, and the cytokinetic ring. These structures play important roles in polarity, adhesion, and cytokinesis (Chang, 1999; Chang et al., 1997; Evangelista et al., 1997; Evangelista et al., 2002; Sagot et al., 2002a; Tomimaga et al., 2000; Watanabe et al., 1999). Recently, the *Drosophila* protein Spire, which is necessary for proper

fly development, was also shown to nucleate filaments (Quinlan et al., 2005).

The Rho GTPases Cdc42, Rac, and Rho play important roles in controlling the activities of Arp2/3 complex and formins and, in doing so, control actin dynamics in a variety of processes (Pollard and Borisy, 2003; Wallar and Alberts, 2003; Zigmond, 2004). Cdc42 and Rac activate Arp2/3 complex through the intermediacy of WASP family proteins (Pollard and Borisy, 2003). WASP and its relatives bind directly (for Cdc42) or indirectly (for Rac) to the active (GTP bound) forms of the GTPases and to Arp2/3 complex, enabling control of the spatial and temporal dynamics of actin by the dynamics of GTPase signaling. Rho can directly bind and activate the two best-understood members of the formin family: yeast Bni1p and mammalian mDia1 (Kohno et al., 1996; Watanabe et al., 1997). Although the structural and biochemical mechanisms underlying the communication from Cdc42 to WASP to Arp2/3 complex have been extensively studied, much less is known about the physical basis of formin function and regulation.

All formins contain a conserved formin homology 2 (FH2) domain that mediates interactions with actin (Otomo et al., 2005; Wallar and Alberts, 2003; Zigmond, 2004). This domain has a variety of functions in different members of the formin family, including nucleation of new filaments (Evangelista et al., 2002; Harris et al., 2004; Kovar et al., 2003; Li and Higgs, 2003; Pruyne et al., 2002; Sagot et al., 2002b), binding the fast-growing filament barbed end (Harris et al., 2004; Kovar et al., 2003; Kovar and Pollard, 2004; Li and Higgs, 2003; Moseley et al., 2004; Pruyne et al., 2002), inhibition of barbed end-capping proteins (Harris et al., 2004; Li and Higgs, 2003; Moseley et al., 2004; Pring et al., 2003; Zigmond et al., 2003), and filament severing (Harris et al., 2004). In the DRFs, the FH2 domain is immediately followed by a ~30 residue sequence termed the DAD. The DAD binds to a ~500 residue N-terminal regulatory element, causing autoinhibition of FH2 activity through an unknown mechanism (Alberts, 2001; Li and Higgs, 2003; Watanabe et al., 1999). In the DRF mDia1, binding of the RhoA GTPase to this element causes dissociation of DAD peptides (Watanabe et al., 1999) and activation of FH2-DAD proteins in actin assembly assays (Li and Higgs, 2003). Although there may be other activators that act through distinct mechanisms (Li and Higgs, 2003), displacement of DAD from the N terminus is a central feature of DRF activation by Rho.

The mDia1 N terminus has historically been considered to contain three sequence regions: a GTPase binding domain (GBD), which binds RhoA, an FH3 domain, which is found throughout the formin family, and a predicted coiled coil (Higgs and Peterson, 2005; Wallar and Alberts, 2003). Recent biochemical analyses have more clearly identified several functional domains in the N terminus (Li and Higgs, 2005) (Figure 1A). Residues 73–131 (referred to here as the G region, for GTPase binding) are required for RhoA binding and for RhoA-mediated activation of autoinhibited mDia1, but

\*Correspondence: mrosen@biochem.swmed.edu

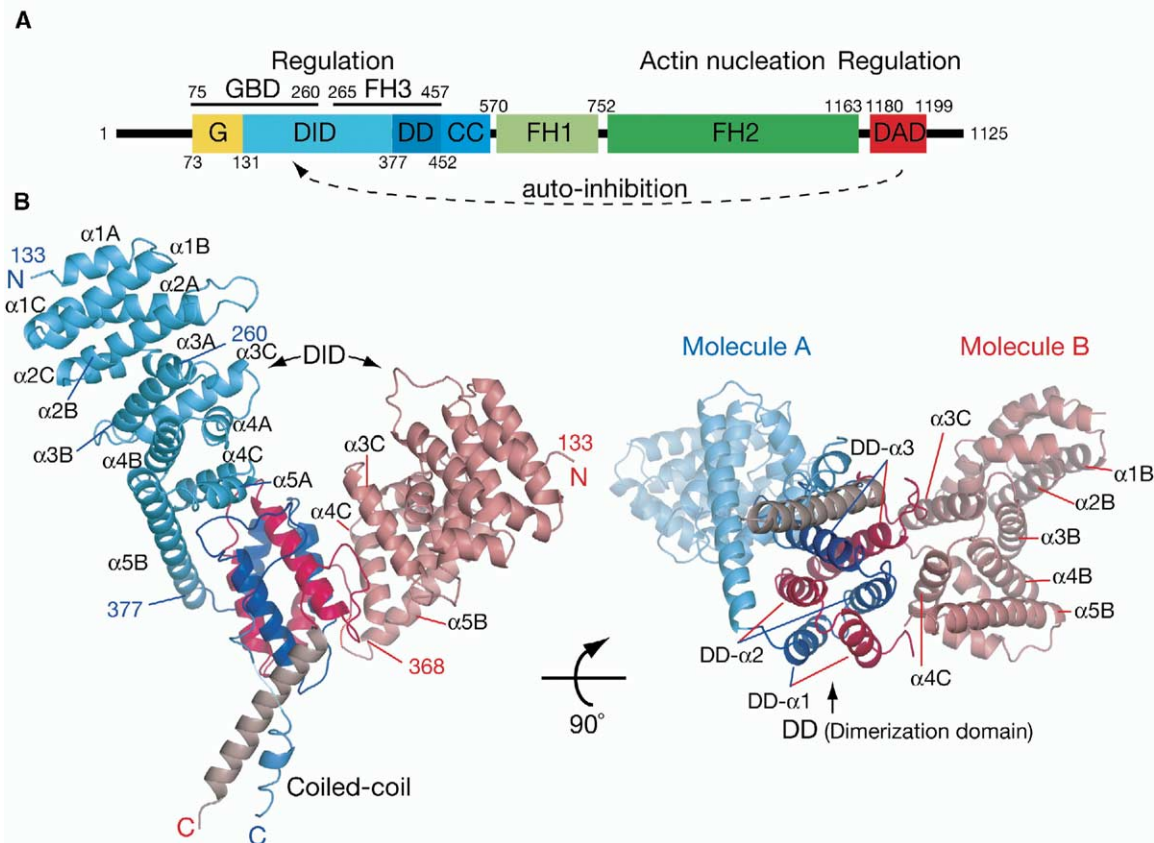


Figure 1. Domain Organization of mDia1

(A) Structural and functional domains of mDia1. Abbreviations: G, GTPase binding region necessary for RhoA binding; DID, Diaphanous inhibitory domain; DD, dimerization domain; CC, coiled coil; FH1, formin homology 1 domain; FH2, formin homology 2 domain; DAD, Diaphanous autoinhibitory domain; GBD, previously described GTPase binding domain; and FH3, formin homology 3 domain. The GBD and FH3 domain are based on sequence conservation and do not correspond to domain boundaries in the structure.

(B) Structure of the dimeric N-terminal regulatory domain of mDia1. Molecule A is light blue (DID) and dark blue (DD, coiled coil). Molecule B is pink (DID) and red (DD, coiled coil). Figures were made with PyMol (DeLano, 2002).

not for autoinhibition. A DID (residues 131–377) binds the DAD and is sufficient to block FH2 activity. A dimerization domain (DD, residues 377–452) is sufficient to cause dimerization of N-terminal mDia1 fragments. A coiled coil immediately follows the DD but is not required for dimerization (see below).

Here, we describe the crystal structure of the minimal dimeric autoinhibitory fragment of the mDia1 N terminus, containing the DID and DD elements plus a short segment of the coiled coil. The DD is composed of an unusual, intertwined six-helix bundle with an  $\sim 2$ -fold symmetry axis. Each DID element consists of a superhelix of five armadillo repeats. In the crystal, the two DIDs project from the DD in an asymmetric manner. NMR and biochemical analyses of a series of N-terminal constructs indicate that the RhoA- and DAD-interaction sites partially overlap on the surface of the DID, suggesting a mechanism for their competitive binding and thus RhoA activation of mDia1. Comparison of mDia1 with other well-characterized GTPase effectors reveals a common autoinhibitory construction

that may be widely used throughout GTPase signaling systems.

## Results and Discussion

### Structure of the mDia1 Autoinhibitory Domain

We determined the crystal structure of an mDia1 fragment containing the DID and DD elements and a portion of the predicted coiled coil (Table 1). This construct (DID-DD, residues 131–516) crystallizes with a dimer in the asymmetric unit. The dimer is organized around the globular DD, from which protrude two structurally independent DID elements in one direction and a short segment of coiled coil in the other direction (Figure 1B).

Each DD monomer contributes three helices (DD- $\alpha 1$ ,  $\alpha 2$ , and  $\alpha 3$ ) to form an antiparallel six-helix bundle with C-terminal loops connecting to the coiled coil (Figure 1B). The structures of the two chains in the bundle are highly similar (0.58 Å backbone rmsd for residues 379–433) and are related by a  $\sim 2$ -fold symmetry axis perpendicular to the helices (vertical in Figure 1B, right).

Table 1. Data Collection, Structure Determination, and Refinement

Data Collection		
Crystal	Native	SeMet <sup>a</sup>
Energy (eV)	12657.4	12657.4
Resolution range (Å)	46.00–2.40 (2.44–2.40)	46.04–3.00 (3.05–3.00)
Unique reflections	61,323 (3,029)	61,876 (3,086)
Multiplicity	5.9 (4.5)	3.1 (3.2)
Data completeness (%)	99.8 (97.6)	99.7 (100.0)
R <sub>merge</sub> (%) <sup>b</sup>	6.3 (56.7)	6.1 (35.8)
I/σ (I)	27.3 (2.1)	26.5 (4.7)
Wilson B value (Å <sup>2</sup> )	57.1	77.9
Phase Determination		
Anomalous scatterer	Selenium (28 of 38 possible sites)	
Figure of merit (46.0–3.00 Å)	0.36	
Refinement Statistics		
Resolution range (Å)	20.0–2.40	
Number of reflections R <sub>work</sub> /R <sub>free</sub>	59,657/1542	
Atoms (non-H protein/solvent)	5437/251	
R <sub>work</sub> (%)	19.8	
R <sub>free</sub> (%)	23.4	
Rmsd bond length (Å)	0.020	
Rmsd bond angle (°)	1.744	
Mean B value (Å <sup>2</sup> )	55.4	
Missing residues	Molecule 1 (131–132, 457–461, 475–516) Molecule 2 (131–132, 373–375, 475–516)	

Data for the outermost shell are given in parentheses.

<sup>a</sup>Bijvoet pairs were kept separate for data processing.

<sup>b</sup>R<sub>merge</sub> = 100  $\sum_h \sum_i |I_{h,i} - \langle I_h \rangle| / \sum_h \sum_i I_{h,i}$ , where the outer sum (h) is over the unique reflections and the inner sum (i) is over the set of independent observations of each unique reflection.

The chains interact in an unusual fashion, with the three helices from each chain interlocked. Topologically, they cannot be separated without dissociation of either the N- or C-terminal helix from at least one chain. This interwoven architecture suggests that the N-terminal domain is likely to be a constitutive dimer and may only dissociate through (partial) unfolding.

Two ~20 residue helices associated into a coiled coil emerge from one face of the DD and are aligned approximately parallel to its long axis (Figure 1B). These helices are attached asymmetrically to the DD. In molecule A, this helix is antiparallel to DD-α3 and thus attaches through a loop that starts at the opposite end of the structure and extends across nearly the entire domain before encountering its partner. In molecule B, this helix is parallel to DD-α3 and attaches through a loop confined to the base of the bundle. Based on sequence analyses, the paired helices observed in the crystal are likely only a portion of a much longer (~120 residue) coiled coil in the full-length protein (Higgs and Peterson, 2005; Lupas et al., 1991).

The DID is composed of five armadillo repeats (Groves and Barford, 1999) of two or three helices each stacked together to form an elongated superhelical domain (Figure 1B). Successive repeats are displaced from one another by ~15–20° rotations, giving the structure an overall superhelical twist of ~90°. The B helices in each domain stack in a twisted ladder-like arrangement to form a concave face of the superhelix (see molecule B, Figure 1B). The opposite convex face is formed by stacking of helices A and C. The two DIDs

in the asymmetric unit are very similar (backbone rmsd = 0.57 Å, residues 133–370), but their interactions with the DD are different; a ~2-fold axis relating the DIDs (approximately vertical in Figure 1A, left) is nearly orthogonal to that relating the two chains in the DD. The DID of molecule A, through its helices α4C, α5A, and α5B, contacts its own C-terminal loop and DD-α2 of molecule B in the DD. The DID of molecule B, through helices α3C, α4C, and α5B, makes more extensive contacts with the DD, involving its own C-terminal loop and DD-α3, as well as DD-α2 of molecule A. These interactions position the two DIDs with their convex surfaces directed toward one another and their concave surfaces directed outward.

The previously described GBD and FH3 sequence boundaries do not demarcate domain boundaries in the structure (Figure 1A) (Bateman et al., 2002). The GBD (residues 75–260) is composed of 70 residues N-terminal to the first armadillo repeat plus the first two armadillo repeats. The FH3 domain (residues 265–457) contains armadillo repeats three to five of each DID plus the DD. Phylogenetic analyses of the formin family have identified two conserved N-terminal sequences, termed N1 and N2, of ~30 and 15 residues, respectively, that are present in many members (Higgs and Peterson, 2005). These sequences constitute portions of armadillo repeats one and two (N1) and two (N2) in the structure, suggesting that the armadillo repeats may be a common element of the N-terminal domains across the family.

It is unclear whether the asymmetry of the interac-

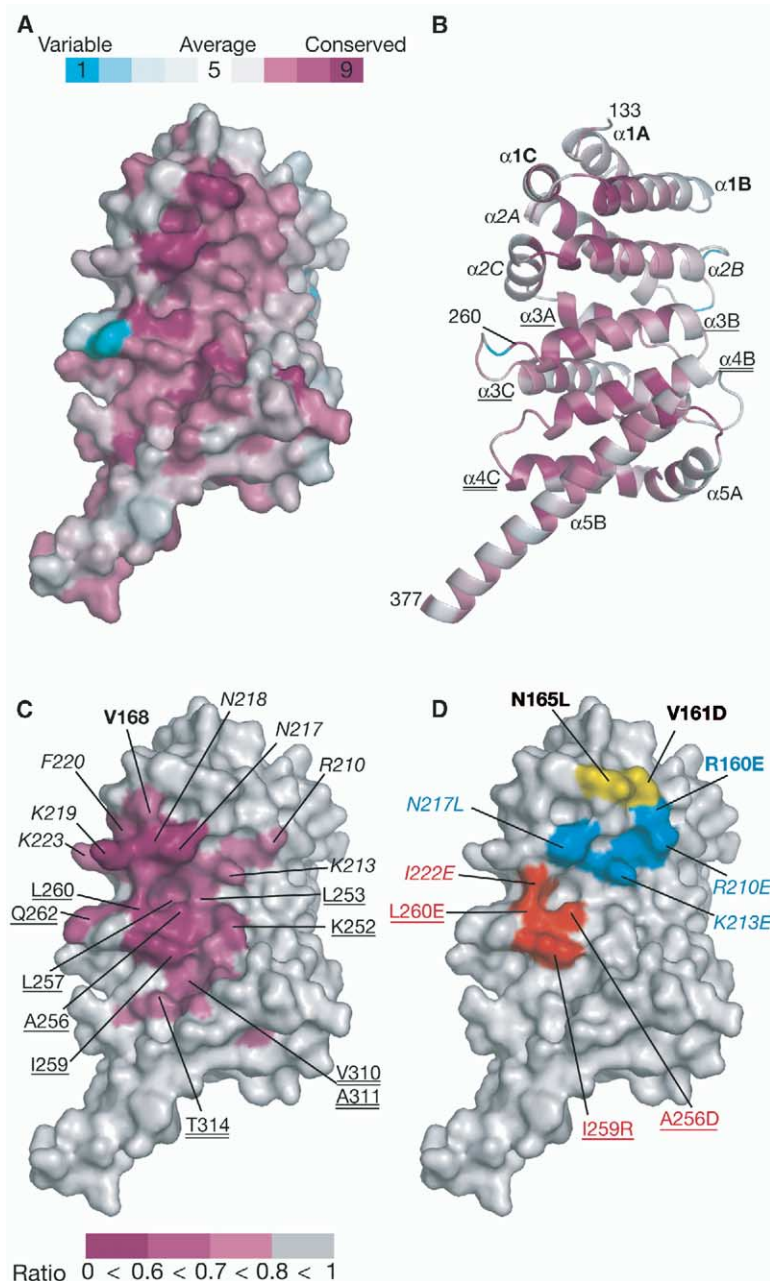


Figure 2. Functional Surfaces of the DID

(A and B) Surface and ribbon representation of the DID, colored according to conservation in the Dia, FRL, and DAAM forms (blue→white→red with increasing conservation) (Glaser et al., 2003).

(C) DAD binding site on the DID surface identified by NMR cross saturation and colored by ratio of saturated to nonsaturated NMR peak intensities.

(D) DID surface colored according to effects of mutations on RhoA binding and FH2-inhibitory activity. Red, mutations decrease inhibitory activity only; yellow, mutations decrease RhoA affinity only; and blue, mutations decrease both inhibitory activity and RhoA affinity. In (B), (C), and (D), residues in armadillo repeats one, two, three, and four are labeled with bold, italic, single underline, and double underline, respectively.

tions between the DID and DD observed in the crystal is preserved in solution. The two DIDs are structurally independent. They should be able to sample both conformations unless there is significant cooperativity communicated through the DD. Conformational transitions between the two orientations, perhaps controlled by binding partners, could play a role in DRF regulation. Alternatively, the asymmetry may be a consequence of crystallization, with only one of the two observed orientations highly populated in solution. In either scenario, the key functional surfaces of the DID described below should be accessible to binding partners.

To identify potential functionally important sites in the DID, we performed a structure-based sequence align-

ment of the N-terminal domains of the 20 DRFs in the Diaphanous, FRL, and DAAM groups, which are believed to be regulated through an autoinhibitory mechanism similar to mDia1 (Higgs and Peterson, 2005) (Figure S1 available with this article online). Mapping conservation onto the structure reveals a single patch on the concave surface of the DID containing the B helices from all five armadillo repeats (Figures 2A and 2B). Highest surface conservation is observed near the C termini of helices  $\alpha$ 1B,  $\alpha$ 2B, and  $\alpha$ 3B. Residues on the exposed convex surface of the DID are not conserved, suggesting that the common functions of the N-terminal regions are mediated by the concave side of the domain.

**RhoA and DAD Binding Sites Partially Overlap**

To gain insight into the mechanisms of autoinhibition and GTPase activation, we examined the binding of a series of N-terminal constructs to the DAD peptide and RhoA. A long, dimeric construct (G-DID-DD, residues 73–516) contains the elements observed in the crystal plus N-terminal residues necessary to bind RhoA with high affinity (Li and Higgs, 2005). We also generated monomeric versions of these constructs, which lack the DD and CC (G-DID, DID: residues 73–370 and 131–370, respectively [Li and Higgs, 2005]). We tested whether the monomeric and dimeric proteins bind the ligands RhoA and DAD in a similar manner and whether the binding is cooperative. A fluorescence assay for binding of RhoA-GMPPNP (a RhoA-GTP analog) yielded dissociation constants ( $K_D$ s) of 0.24  $\mu$ M and 0.32  $\mu$ M for the G-DID and G-DID-DD proteins, indicating the absence of cooperative binding in the dimer. A  $K_D$  of 0.25  $\mu$ M has been reported for a dimeric DID-DD construct binding to a monomeric DAD peptide (Li and Higgs, 2005). This affinity is weaker than the inhibitory potency observed for DID-DD proteins in FH2-mediated actin assembly assays, likely because of the bivalency effect of the dimeric N terminus binding to the dimeric FH2-DAD protein used in the assays (Li and Higgs, 2003). We have not quantified the affinity of the monomeric DID for DAD peptide. However, the complex does not dissociate during size exclusion chromatography, and the binding interaction is in slow exchange on the NMR chemical shift timescale (data not shown), suggesting that the  $K_D$  for the monomeric DID is probably in the micromolar or smaller range. Thus, the monomeric DID and G-DID bind DAD and RhoA similarly to the dimeric constructs, indicating the absence of cooperative binding in the dimers. Because the monomeric proteins are much more amenable to NMR analyses, we used these constructs to examine the interactions of the mDia1 N terminus with ligands.

$^1\text{H}/^{15}\text{N}$  TROSY HSQC spectra (Pervushin et al., 1997) of the DID and G-DID proteins are both of high quality, showing >95% of the expected backbone amide resonances (Figure 3A). Peaks in the DID spectra are largely a subset of those in the G-DID spectra, with average deviations of  $0.002 \pm 0.002$  and  $0.008 \pm 0.008$  ppm in  $^1\text{H}$  and  $^{15}\text{N}$  chemical shifts for the 197 nonoverlapped shared peaks. Additional peaks in the G-DID spectra show increased intensity over those corresponding to the DID. Together, these data indicate that in the absence of RhoA, the N-terminal G region is structurally independent from the armadillo repeats of the DID and likely mobile in solution. Several amide  $^1\text{H}$  chemical shifts from the G region are downfield shifted to  $\sim 9$  ppm, indicating persistent hydrogen bonding and thus structural order in this element.

We used two independent methods to identify the DAD binding site on the DID. NMR cross saturation reveals direct contacts between a protonated ligand and its fully deuterated binding partner (Takahashi et al., 2000). Cross saturation from a protonated DAD peptide to deuterated DID revealed contacts to a contiguous patch on the concave surface of the DID composed of  $\alpha 2\text{B}$ ,  $\alpha 2\text{C}$ ,  $\alpha 3\text{B}$ , the  $\alpha 3\text{B}$ – $\alpha 3\text{C}$  loop, and  $\alpha 4\text{B}$  (Figures 2C and 3B). This patch spans much of the conserved surface of the DID (Figure 2), except for  $\alpha 1\text{B}$  and the N

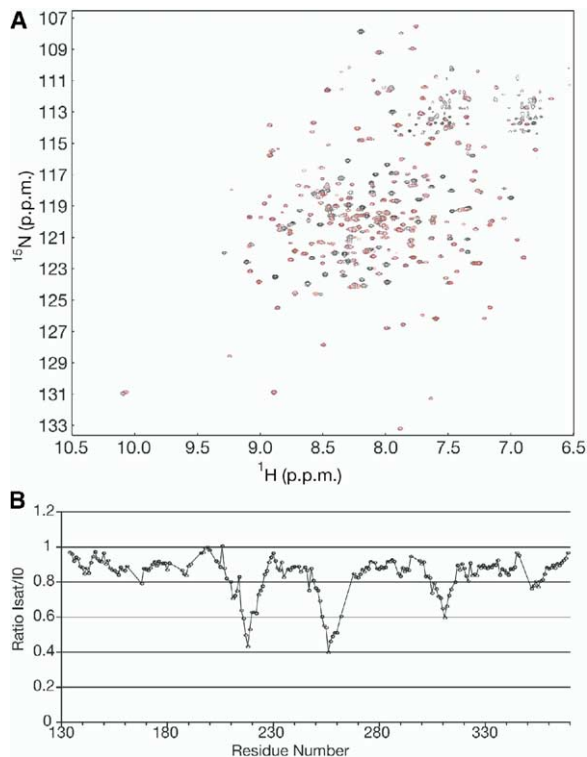


Figure 3. NMR Analyses of DID and G-DID

(A) Overlay of  $^1\text{H}/^{15}\text{N}$  TROSY HSQC spectra of DID (red) and G-DID (black).

(B) Cross saturation from a protonated DAD peptide to deuterated DID. The ratio for each residue was calculated as described in the Experimental Procedures.

terminus of  $\alpha 2\text{B}$ . Interaction between DAD and DID is necessary for high-potency autoinhibition in mDia1 (Wallar and Alberts, 2003). Thus, we prepared a series of mutants in the G-DID-DD protein and studied their ability to inhibit actin assembly by an mDia1 FH2-DAD construct. As shown in Figure 4A, the mDia1 FH2-DAD protein has strong actin assembly activity that can be repressed by wild-type (wt) G-DID-DD. Mutations in the  $\alpha 2\text{B}$ – $\alpha 2\text{C}$  loop and  $\alpha 3\text{B}$  decreased the inhibitory potency of G-DID-DD most significantly (Figures 2D and 4A). Smaller effects were also observed for mutations in  $\alpha 2\text{B}$  and  $\alpha 1\text{B}$ , but only one of four mutations in the latter decreased inhibitory potency. In all cases, inhibitory activity of the mutants correlated with direct binding of the proteins to an immobilized DAD peptide (Figure 4C). The NMR and biochemical data are consistent in identifying a DAD binding site on the concave surface of the DID spanning armadillo repeats two, three, and four.

The large size ( $\sim 50$  kDa) and poor chemical shift dispersion of the complex of G-DID with RhoA prevented us from obtaining reliable chemical shift assignments of this system. Thus, we used only mutagenesis to map the RhoA contacts with mDia1. Mutation of residues in  $\alpha 1\text{B}$  and  $\alpha 2\text{B}$  reduced the affinity of RhoA for G-DID-DD more than 35-fold, with some causing effects comparable to elimination of the G region (Figures 2D and

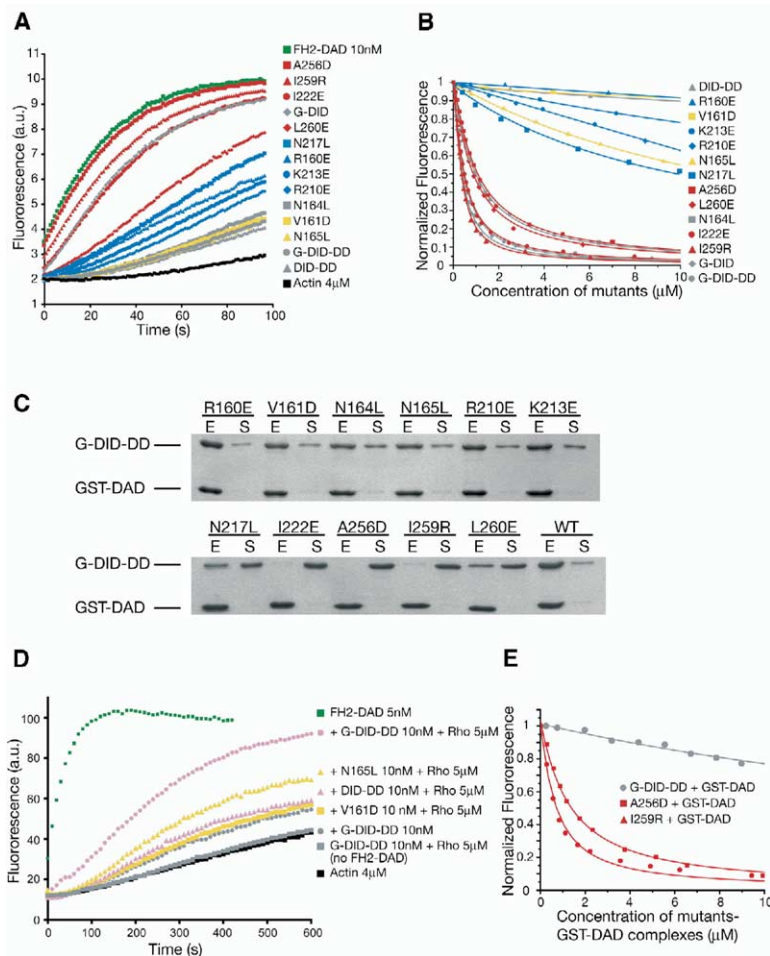


Figure 4. Biochemical Characterization of Effects of Point Mutations in mDia1 G-DID-DD Protein

(A) Effects of mutations on inhibitory activity monitored by actin assembly assay (indicated by increase in fluorescence of pyrene-actin on polymerization) using 10 nM FH2-DAD and 20 nM G-DID-DD mutants.

(B) Effects of mutations on RhoA binding monitored by changes in fluorescence of Mant-GMPPNP-RhoA upon addition of G-DID-DD mutants. The decrease in fluorescence indicates RhoA binding. In panels (A) and (B), data are colored according to Figure 2D.

(C) Binding of G-DID-DD mutants to an immobilized GST-DAD peptide. S and E stand for supernatant and glutathione elution of bound proteins, respectively.

(D) Activation of FH2-DAD by RhoA. Inhibition of 5 nM FH2-DAD-mediated actin assembly by 10 nM G-DID-DD mutants was relieved by 5  $\mu$ M RhoA-GMPPNP.

(E) Competitive binding of G-DID-DD mutants to RhoA in the presence of GST-DAD. Equimolar G-DID-DD mutants and GST-DAD were mixed and titrated into 0.3  $\mu$ M Mant-GMPPNP-RhoA. All data are representative of at least two independent measurements.

4B, and Table 2). In contrast, mutations in  $\alpha$ 3B had virtually no effect on affinity (<3-fold). Thus, RhoA makes energetically favorable interactions with the C-terminal portions of  $\alpha$ 1B and  $\alpha$ 2B and likely directly contacts these elements and/or proximal structures.

Our data indicate that both DAD and RhoA interact with  $\alpha$ 2B. This structural overlap of the DID contact

sites likely contributes strongly to the displacement of DAD by RhoA and thus to RhoA activation of mDia1.

We performed two additional experiments to confirm our mapping and directly examine negative cooperativity between RhoA and DAD binding to DID. As shown in Figure 4D, RhoA-GMPPNP partially relieves the inhibitory activity of G-DID-DD on FH2-DAD-mediated actin assembly, as previously reported (Li and Higgs, 2003). Mutant G-DID-DD proteins that have weak affinity for RhoA (V161D and N165L) still repress FH2 activity comparable to wt. However, RhoA activation of these mutants is much poorer, confirming that RhoA contact sites on the DID are needed for activation by the GTPase. We also examined RhoA affinity for G-DID-DD in the presence of GST-DAD proteins (Figure 4E). For G-DID-DD mutants that are severely impaired in DAD binding (A256D and I259R), RhoA affinity is nearly identical in the presence and absence of GST-DAD (1.2  $\mu$ M versus 0.87  $\mu$ M and 0.57  $\mu$ M versus 0.19  $\mu$ M, respectively). However, for wt G-DID-DD, stoichiometric GST-DAD (which is dimeric and binds G-DID-DD very tightly due to bivalency) reduces RhoA affinity substantially. Thus, the DAD contact sites on the DID are necessary for negative cooperativity between DAD and RhoA. We note that the Mant-GMPPNP-loaded RhoA used in this binding assay likely has a lower affinity for

Table 2. Affinity of RhoA-GMPPNP for mDia1 Fragments

Protein	$K_D$ ( $\mu$ M)
G-DID-DD	0.32 $\pm$ 0.02
DID	Too weak to quantify
G-DID	0.24 $\pm$ 0.02
R160E	Too weak to quantify
V161D	Too weak to quantify
N164L	0.84 $\pm$ 0.02
N165L	16.8 $\pm$ 0.4
R210E	Too weak to quantify
K213E	Too weak to quantify
N217L	12.5 $\pm$ 0.7
I222E	0.34 $\pm$ 0.02
A256D	0.87 $\pm$ 0.04
I259R	0.19 $\pm$ 0.02
L260E	0.73 $\pm$ 0.04

All mutants are in G-DID-DD protein.

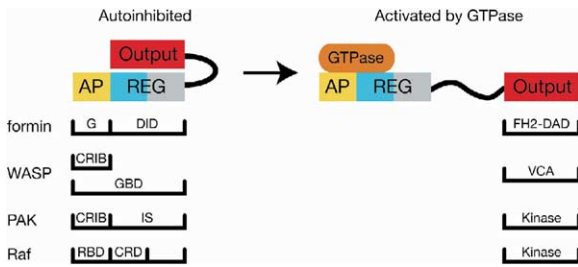


Figure 5. A Common Autoinhibitory Construction of Ras Superfamily GTPase Effectors

Abbreviations: AP, access point and REG, regulatory element. Activity of the mDia1 FH2 domain is negatively regulated through interactions with the DID that are enhanced by DAD (Li and Higgs, 2005). GTPase binding requires the exposed G region also. Activity of the WASP VCA domain is inhibited through binding to the C-terminal segment of the GBD (Kim et al., 2000). GTPase binding requires the exposed CRIB motif. Activity of the Pak kinase domain is inhibited through binding to the inhibitory switch (IS) region (Lei et al., 2000). GTPase binding requires the exposed CRIB motif. Activity of the Raf kinase domain is inhibited by intramolecular interactions of the cysteine-rich domain (Williams et al., 2000), whereas GTPase activation requires the independent Ras binding domain (RBD).

G-DID proteins than the GMPPNP-loaded RhoA used in the activity assays, based on precedent with Cdc42 (Leung and Rosen, 2005; Rudolph et al., 2001). Thus, RhoA-GMPPNP can partially activate in the assays, but RhoA-Mant-GMPPNP does not bind appreciably at similar concentrations.

### A Common Autoinhibitory Construction of GTPase Effectors

Many effectors of Ras superfamily GTPases are regulated by autoinhibition. The physical mechanisms of inhibition and GTPase-mediated activation are best understood for the effectors WASP (Kim et al., 2000), Pak (Lei et al., 2000), Raf (Williams et al., 2000), and mDia1, where the structures and energetics of the inhibited and activated forms have been examined more closely. Each protein has an activity-bearing (output) domain that is inhibited through direct binding to a distinct regulatory element (Figure 5). GTPase contacts to the regulatory domain are believed to displace it from the output domain, providing the core route to effector activation. In all cases, GTPase binding requires an additional, structurally independent domain that is immediately adjacent to the regulatory domain. This domain, which we refer to as an access point, does not participate itself in inhibition of the output domain but makes important contacts to the GTPase that are necessary for effector activation. Thus, the GTPase binding element is bipartite, spanning the regulatory domain and the exposed access point. Conservation of this construction across four unrelated effectors suggests either ease of evolutionary development or evolutionary pressure on some functional consequence. We have recently shown that the exposed CRIB motif of WASP allows the GTPase Cdc42 to bind in its GDP form without causing complete disruption of the GBD-VCA regulatory interaction. Thus, the Cdc42 nucleotide switch

modulates the thermodynamic coupling between the GTPase binding and allosteric equilibria in WASP, a property that may enhance signaling fidelity in crowded membrane environments (Leung and Rosen, 2005). Access point construction may in general facilitate evolution of different degrees of thermodynamic coupling between GTPase binding equilibria and regulatory equilibria in effectors. This could enable development of some effectors that can be fully activated by saturating GTP-GTPase alone (e.g., WASP) (Leung and Rosen, 2005; Prehoda and Lim, 2002) and others where saturating GTPase can only partially activate (e.g., mDia1) (Li and Higgs, 2003), necessitating cooperative activation through multiple inputs *in vivo*. It is also possible that access points may provide a more efficient kinetic pathway to effector activation, with initial GTPase binding to the exposed element allowing release of the regulatory element to occur in unimolecular fashion. The potential importance of these and other functional consequences of access point construction will be clarified as more GTPase-effector systems are analyzed in biochemical detail.

### Experimental Procedures

#### Protein Preparation and Crystallization

Proteins were expressed in *E. coli* BL21(DE3) and purified chromatographically. The mDia1 DID-DD construct (residues, 131–516) was crystallized at 20°C in 100 mM Hepes (pH 7.25), 9% (w/v) PEG3550 by hanging drop vapor diffusion. Crystals grew to 120 × 120 × 200 μm in one week and were cryo-protected with 100 mM Hepes (pH 7.25), 11.5% (w/v) PEG3550, and 35% (v/v) ethylene glycol and flash cooled in liquid propane. Crystals exhibit the symmetry of space group P3<sub>2</sub> with cell dimensions of a = 121.57 Å, b = 121.57 Å, and c = 94.89 Å and contain two molecules in the asymmetric unit.

#### Crystallographic Data Collection and Structure Determination

Diffraction data were collected at beamline 19-ID (SBC-CAT) at the Advanced Photon Source (Argonne National Laboratory, Argonne, Illinois, USA) and processed with HKL2000 (Otwinowski and Minor, 1997). Phases were calculated from a single-wavelength anomalous dispersion (SAD) experiment at the selenium peak by using the selenomethionine variant of mDia1. By using diffraction data to 3.0 Å, 28 of 38 possible selenium sites were located, refined, and subjected to density modification with the program CNS (Brunger et al., 1998). A native dataset was collected to a resolution of 2.4 Å and used for model building (program O [Jones et al., 1991]) and refinement (Refmac5 [Murshudov et al., 1997]), resulting in an R<sub>work</sub> of 21.7% and an R<sub>free</sub> of 24.9%. The quality of the electron density did not allow the unambiguous identification of side chains in the C-terminal portion of one of the mDia1 molecules (residues 462–474). Data collection and refinement statistics are shown in Table 1.

#### Biochemical Analyses

Assembly of 4 μM actin (5% pyrene labeled) in the presence of mDia1 FH2-DAD (745–1209), various constructs of mDia1 N terminus proteins, and RhoA-GMPPNP were performed as reported (Li and Higgs, 2003). Mant-GMPPNP was synthesized as reported (Hiratsuka, 1983) and loaded on RhoA (residues 1–181) by incubation with 5 mM EDTA for 3 hr at 25°C and quenched by addition of 10 mM MgCl<sub>2</sub>. mDia1 was titrated into 0.3 μM RhoA-Mant-GMPPNP in 50 mM KCl, 1 mM MgCl<sub>2</sub>, 1 mM EGTA, and 10 mM imidazole (pH 7.0) and affinity determined from the quench in Mant fluorescence (Rudolph et al., 1998). To examine interactions between DAD and G-DID-DD proteins, 500 pmol of GST-DAD was immobilized on glutathione-Sepharose beads (Amersham). 500 pmol of G-DID-DD protein (wt or mutant) was added to the beads in 10 mM Hepes (pH 7.0), 150 mM NaCl. Beads were washed and

the complex was eluted with 10 mM glutathione. Only 10 pmol of GST-DAD was loaded onto SDS-page.

#### NMR Spectroscopy

Backbone  $^1\text{H}$ ,  $^{15}\text{N}$ ,  $^{13}\text{C}\alpha$ , and  $^{13}\text{C}\beta$  assignments of DID ( $^2\text{H}/^{13}\text{C}/^{15}\text{N}$ ) bound to DAD ( $^1\text{H}$ ) were obtained by using TROSY versions of CT-HNCA, CT-HN(CO)CA, HN(CA)CB, HN(CO)CACB, HNCO, and HN(CA)CO experiments (Yang and Kay, 1999). Cross-saturation experiments (Takahashi et al., 2000) were performed on samples in 90%  $\text{H}_2\text{O}/10\%$   $\text{D}_2\text{O}$ . Saturation of the aliphatic protons of the DAD peptide was achieved with a train of CHIRP adiabatic pulses, each with a maximum RF amplitude of 125 Hz and duration of 40 ms (the adiabatic factor  $Q_0 = 2.45$ ) and excitation centered at 1.2 ppm, providing a  $\sim 1600$  Hz irradiated bandwidth for a total of 1 s prior to initiation of a TROSY-HSQC pulse sequence (Pervushin et al., 1997). The relaxation delay was set to 2 s. The reference spectrum was taken with the same experimental setup, except the center for the adiabatic pulse was shifted to  $-20,000$  Hz off resonance. Total acquisition time was 7.5 hr for each spectrum. The ratio of the intensity for each peak between the cross-saturated and the reference spectrum was calculated. Peaks with a ratio  $<0.8$  were considered to show cross saturation. We confirmed that these experimental conditions do not produce significant artifacts from cysteine residues by comparison with a free G-DID ( $^2\text{H}/^{13}\text{C}/^{15}\text{N}$ ) sample in 90%  $\text{H}_2\text{O}/10\%$   $\text{D}_2\text{O}$ . Spectra were processed with the program nmrPipe (Delaglio et al., 1995) and analyzed by using nmrPipe and nmrview (Johnson and Blevins, 1994).

#### Supplemental Data

Supplemental Data include one figure and are available online with this article at <http://www.molecule.org/cgi/content/full/18/3/273/DC1>.

#### Acknowledgments

We thank Sandra Hill and Chad Brautigam for excellent technical assistance, Toshio Yamazaki for assistance in NMR experiments, Lewis Kay for providing pulse sequences, and Kentaro Ihara for advice on preparation of RhoA. This work was supported by National Institutes of Health grants GM56322 and GM066311. T.O. was supported by the Human Frontier Science Program. Use of the Argonne National Laboratory Structural Biology Center beamlines at the Advanced Photon Source was supported by the U.S. Department of Energy, Office of Energy Research, under Contract Number W-31-109-ENG-38. This investigation was conducted in a facility constructed with support from the Research Facilities Improvement Program Grant Number C06 RR-15437.

Received: March 17, 2005

Revised: March 31, 2005

Accepted: April 5, 2005

Published online: April 14, 2005

#### References

Alberts, A.S. (2001). Identification of a carboxyl-terminal diaphanous-related formin homology protein autoregulatory domain. *J. Biol. Chem.* **276**, 2824–2830.

Bateman, A., Birney, E., Cerruti, L., Durbin, R., Etwiller, L., Eddy, S.R., Griffiths-Jones, S., Howe, K.L., Marshall, M., and Sonnhammer, E.L. (2002). The Pfam protein families database. *Nucleic Acids Res.* **30**, 276–280.

Brunger, A.T., Adams, P.D., Clore, G.M., DeLano, W.L., Gros, P., Grosse-Kunstleve, R.W., Jiang, J.S., Kuszewski, J., Nilges, M., Pannu, N.S., et al. (1998). Crystallography & NMR system: a new software suite for macromolecular structure determination. *Acta Crystallogr. D Biol. Crystallogr.* **54**, 905–921.

Carlier, M.F., Le Clainche, C., Wiesner, S., and Pantaloni, D. (2003). Actin-based motility: from molecules to movement. *Bioessays* **25**, 336–345.

Chang, F. (1999). Movement of a cytokinesis factor cdc12p to the site of cell division. *Curr. Biol.* **9**, 849–852.

Chang, F., Drubin, D., and Nurse, P. (1997). cdc12p, a protein required for cytokinesis in fission yeast, is a component of the cell division ring and interacts with profilin. *J. Cell Biol.* **137**, 169–182.

Delaglio, F., Grzesiek, S., Vuister, G.W., Zhu, G., Pfeifer, J., and Bax, A. (1995). NMRPipe: a multidimensional spectral processing system based on UNIX pipes. *J. Biomol. NMR* **6**, 277–293.

DeLano, W.L. (2002). The PyMOL User's Manual (San Carlos, CA: DeLano Scientific).

Evangelista, M., Blundell, K., Longtine, M.S., Chow, C.J., Adames, N., Pringle, J.R., Peter, M., and Boone, C. (1997). Bni1p, a yeast formin linking cdc42p and the actin cytoskeleton during polarized morphogenesis. *Science* **276**, 118–122.

Evangelista, M., Pruyne, D., Amberg, D.C., Boone, C., and Bretscher, A. (2002). Formins direct Arp2/3-independent actin filament assembly to polarize cell growth in yeast. *Nat. Cell Biol.* **4**, 260–269.

Fehrenbacher, K.L., Boldogh, I.R., and Pon, L.A. (2003). Taking the A-train: actin-based force generators and organelle targeting. *Trends Cell Biol.* **13**, 472–477.

Glaser, F., Pupko, T., Paz, I., Bell, R.E., Bechor-Shental, D., Martz, E., and Ben-Tal, N. (2003). ConSurf: identification of functional regions in proteins by surface-mapping of phylogenetic information. *Bioinformatics* **19**, 163–164.

Groves, M.R., and Barford, D. (1999). Topological characteristics of helical repeat proteins. *Curr. Opin. Struct. Biol.* **9**, 383–389.

Harris, E.S., Li, F., and Higgs, H.N. (2004). The mouse formin, FRL-alpha, slows actin filament barbed end elongation, competes with capping protein, accelerates polymerization from monomers, and severs filaments. *J. Biol. Chem.* **279**, 20076–20087.

Higgs, H.N., and Pollard, T.D. (2001). Regulation of actin filament network formation through Arp2/3 complex: activation by a diverse array of proteins. *Annu. Rev. Biochem.* **70**, 649–676.

Higgs, H.N., and Peterson, K.J. (2005). Phylogenetic analysis of the formin homology 2 domain. *Mol. Biol. Cell* **16**, 1–13.

Hiratsuka, T. (1983). New ribose-modified fluorescent analogs of adenine and guanine nucleotides available as substrates for various enzymes. *Biochim. Biophys. Acta* **742**, 496–508.

Johnson, B.A., and Blevins, R.A. (1994). NMRView: a computer program for the visualization and analysis of NMR data. *J. Biomol. NMR* **4**, 603–614.

Jones, T.A., Zou, J.Y., Cowan, S.W., and Kjeldgaard, M. (1991). Improved methods for building protein models in electron density maps and the location of errors in these models. *Acta Crystallogr. A* **47**, 110–119.

Kim, A.S., Kakalis, L.T., Abdul-Manan, N., Liu, G.A., and Rosen, M.K. (2000). Autoinhibition and activation mechanisms of the Wiskott-Aldrich syndrome protein. *Nature* **404**, 151–158.

Kohno, H., Tanaka, K., Mino, A., Umikawa, M., Imamura, H., Fujiwara, T., Fujita, Y., Hotta, K., Qadota, H., Watanabe, T., et al. (1996). Bni1p implicated in cytoskeletal control is a putative target of Rho1p small GTP binding protein in *Saccharomyces cerevisiae*. *EMBO J.* **15**, 6060–6068.

Kovar, D.R., and Pollard, T.D. (2004). Insertional assembly of actin filament barbed ends in association with formins produces piconewton forces. *Proc. Natl. Acad. Sci. USA* **101**, 14725–14730.

Kovar, D.R., Kuhn, J.R., Tichy, A.L., and Pollard, T.D. (2003). The fission yeast cytokinesis formin Cdc12p is a barbed end actin filament capping protein gated by profilin. *J. Cell Biol.* **161**, 875–887.

Lei, M., Lu, W., Meng, W., Parrini, M.C., Eck, M.J., Mayer, B.J., and Harrison, S.C. (2000). Structure of PAK1 in an autoinhibited conformation reveals a multistage activation switch. *Cell* **102**, 387–397.

Leung, D.W., and Rosen, M.K. (2005). The nucleotide switch in Cdc42 modulates coupling between the GTPase-binding and allosteric equilibria of WASP. *Proc. Natl. Acad. Sci. USA* **102**, 5685–5690.

Li, F., and Higgs, H.N. (2003). The mouse Formin mDia1 is a potent

- actin nucleation factor regulated by autoinhibition. *Curr. Biol.* **13**, 1335–1340.
- Li, F., and Higgs, H.N. (2005). Dissecting requirements for auto-inhibition of actin nucleation by the formin, mDia1. *J. Biol. Chem.* **280**, 6986–6992.
- Lupas, A., Van Dyke, M., and Stock, J. (1991). Predicting coiled coils from protein sequences. *Science* **252**, 1162–1164.
- Miletic, A.V., Swat, M., Fujikawa, K., and Swat, W. (2003). Cytoskeletal remodeling in lymphocyte activation. *Curr. Opin. Immunol.* **15**, 261–268.
- Moseley, J.B., Sagot, I., Manning, A.L., Xu, Y., Eck, M.J., Pellman, D., and Goode, B.L. (2004). A conserved mechanism for Bni1- and mDia1-induced actin assembly and dual regulation of Bni1 by Bud6 and profilin. *Mol. Biol. Cell* **15**, 896–907.
- Murshudov, G.N., Vagin, A.A., and Dodson, E.J. (1997). Refinement of macromolecular structures by the maximum-likelihood method. *Acta Crystallogr. D Biol. Crystallogr.* **53**, 240–255.
- Otomo, T., Tomchick, D.R., Otomo, C., Panchal, S.C., Machius, M., and Rosen, M.K. (2005). Structural basis of actin filament nucleation and processive capping by a formin homology 2 domain. *Nature* **433**, 488–494.
- Otwinowski, Z., and Minor, W. (1997). Processing X-ray diffraction data collected in oscillation mode. *Methods Enzymol.* **276**, 307–326.
- Pervushin, K., Riek, R., Wider, G., and Wuthrich, K. (1997). Attenuated T2 relaxation by mutual cancellation of dipole-dipole coupling and chemical shift anisotropy indicates an avenue to NMR structures of very large biological macromolecules in solution. *Proc. Natl. Acad. Sci. USA* **94**, 12366–12371.
- Pollard, T.D., and Borisy, G.G. (2003). Cellular motility driven by assembly and disassembly of actin filaments. *Cell* **112**, 453–465.
- Prehoda, K.E., and Lim, W.A. (2002). How signaling proteins integrate multiple inputs: a comparison of N- and Cdk2. *Curr. Opin. Cell Biol.* **14**, 149–154.
- Pring, M., Evangelista, M., Boone, C., Yang, C., and Zigmond, S.H. (2003). Mechanism of formin-induced nucleation of actin filaments. *Biochemistry* **42**, 486–496.
- Pruyne, D., Evangelista, M., Yang, C., Bi, E., Zigmond, S., Bretscher, A., and Boone, C. (2002). Role of formins in actin assembly: nucleation and barbed-end association. *Science* **297**, 612–615.
- Quinlan, M.E., Heuser, J.E., Kerkhoff, E., and Mullins, R.D. (2005). *Drosophila* Spire is an actin nucleation factor. *Nature* **433**, 382–388.
- Rudolph, M.G., Bayer, P., Abo, A., Kuhlmann, J., Vetter, I.R., and Wittinghofer, A. (1998). The Cdc42/Rac interactive binding region motif of the Wiskott Aldrich syndrome protein (WASP) is necessary but not sufficient for tight binding to Cdc42 and structure formation. *J. Biol. Chem.* **273**, 18067–18076.
- Rudolph, M.G., Linnemann, T., Gruenewald, P., Wittinghofer, A., Vetter, I.R., and Herrmann, C. (2001). Thermodynamics of Ras/effector and Cdc42/effector interactions probed by isothermal titration calorimetry. *J. Biol. Chem.* **276**, 23914–23921.
- Sagot, I., Klee, S.K., and Pellman, D. (2002a). Yeast formins regulate cell polarity by controlling the assembly of actin cables. *Nat. Cell Biol.* **4**, 42–50.
- Sagot, I., Rodal, A.A., Moseley, J., Goode, B.L., and Pellman, D. (2002b). An actin nucleation mechanism mediated by Bni1 and profilin. *Nat. Cell Biol.* **4**, 626–631.
- Takahashi, H., Nakanishi, T., Kami, K., Arata, Y., and Shimada, I. (2000). A novel NMR method for determining the interfaces of large protein-protein complexes. *Nat. Struct. Biol.* **7**, 220–223.
- Tominaga, T., Sahai, E., Chardin, P., McCormick, F., Courtneidge, S.A., and Alberts, A.S. (2000). Diaphanous-related formins bridge Rho GTPase and Src tyrosine kinase signaling. *Mol. Cell* **5**, 13–25.
- Waller, B.J., and Alberts, A.S. (2003). The formins: active scaffolds that remodel the cytoskeleton. *Trends Cell Biol.* **13**, 435–446.
- Watanabe, N., Madaule, P., Reid, T., Ishizaki, T., Watanabe, G., Kakiyama, A., Saito, Y., Nakao, K., Jockusch, B.M., and Narumiya, S. (1997). p140mDia, a mammalian homolog of *Drosophila* diaphanous, is a target protein for Rho small GTPase and is a ligand for profilin. *EMBO J.* **16**, 3044–3056.
- Watanabe, N., Kato, T., Fujita, A., Ishizaki, T., and Narumiya, S. (1999). Cooperation between mDia1 and ROCK in Rho-induced actin reorganization. *Nat. Cell Biol.* **1**, 136–143.
- Weaver, A.M., Young, M.E., Lee, W.L., and Cooper, J.A. (2003). Integration of signals to the Arp2/3 complex. *Curr. Opin. Cell Biol.* **15**, 23–30.
- Williams, J.G., Drugan, J.K., Yi, G.S., Clark, G.J., Der, C.J., and Campbell, S.L. (2000). Elucidation of binding determinants and functional consequences of Ras/Raf-cysteine-rich domain interactions. *J. Biol. Chem.* **275**, 22172–22179.
- Yang, D.W., and Kay, L.E. (1999). TROSY triple-resonance four-dimensional NMR spectroscopy of a 46 ns tumbling protein. *J. Am. Chem. Soc.* **121**, 2571–2575.
- Zigmond, S.H. (2004). Formin-induced nucleation of actin filaments. *Curr. Opin. Cell Biol.* **16**, 99–105.
- Zigmond, S.H., Evangelista, M., Boone, C., Yang, C., Dar, A.C., Sicheri, F., Forkey, J., and Pring, M. (2003). Formin leaky cap allows elongation in the presence of tight capping proteins. *Curr. Biol.* **13**, 1820–1823.

#### Accession Numbers

Atomic coordinates and structure factors have been deposited in the Protein Data Bank under accession code 2bnx.